

Localizing merging black holes with gravitational-wave lensing

Otto A. Hannuksela,^{1,2,*} Thomas E. Collett,^{3,†} Mesut Çalışkan,^{4,‡} and Tjonnie G. F. Li^{5,§}

¹*Nikhef – National Institute for Subatomic Physics,
Science Park, 1098 XG Amsterdam, The Netherlands*

²*Department of Physics, Utrecht University,
Princetonplein 1, 3584 CC Utrecht, The Netherlands*

³*Institute of Cosmology and Gravitation, University of Portsmouth,
Burnaby Rd, Portsmouth, PO1 3FX, UK*

⁴*Kavli Institute for Cosmological Physics, and Department of Physics,
University of Chicago, Chicago, IL 60637, USA*

⁵*Department of Physics, The Chinese University of Hong Kong, Shatin, NT, Hong Kong*

(Dated: April 28, 2020)

* o.hannuksela@nikhef.nl

† thomas.collett@port.ac.uk

‡ mesut@uchicago.edu

§ tgfli@cuhk.edu.hk

We report here a method that can precisely localize a merging black hole. The current gravitational-wave (GW) localization methods rely mainly on merging neutron stars or other sources with electromagnetic (EM) counterparts [1, 2]. However, the scientific targets of merging black holes are entirely different and they allow us to probe exciting properties such as higher-order modes, high redshifts, and the strong field of gravity [3–9]. Unfortunately, the lack of an EM counterpart and the poor sky localization accuracies of the current GW detectors [10] make it generally difficult to localize a merging black hole precisely. However, lensed GWs, whose first observation is predicted in this decade [11–13], could allow us to search for the source through locating its similarly lensed host galaxy. Specifically, a dedicated follow-up of the sky localization of the lensed GW could allow us to identify the lensed host galaxy, and to reconstruct its lens profile. Unfortunately, uniquely identifying the correct host galaxy is challenging, because there are hundreds and sometimes thousands of other lensed galaxies within the sky area spanned by the GW observation [14]. However, by combining the GW information with the lens reconstructions of all the lensed galaxy candidates, we show that one can localize quadruply lensed waves to one or at most a few galaxies with the LIGO/Virgo/Kagra network. Using simulated data, we demonstrate that once the lensed host is identified, the GW source can be localized within the host galaxy, and the system can be used to measure the Hubble constant.

GW events are now regularly detected with laser interferometers [15, 16]. With the current detectors, the source sky localization has typical uncertainties of 100s of square degrees [17]. There are >millions of galaxies in such a large sky area, and tens of thousands of galaxies within the 90% error volume [18–22], making identification of the GW event host galaxy impossible unless there is an electromagnetic (EM) counterpart (as was the case for the binary neutron star GW170817 [1, 2]).¹

If a GW event is strongly lensed and thus multiple imaged,² then its host galaxy must also be lensed. We can thus narrow down our search for the host galaxy to strongly lensed galaxies only. Given that there are much less strongly lensed galaxies than non-lensed galaxies [14], this means that the number of possible hosts is greatly reduced compared to non-lensed GWs.

The typical image separation for strong lensing is less than an arcsecond [14]. Thus, the multiple images appear at essentially the same sky location given the GW detector accuracy. Moreover,

¹ See, however, the possibility of identifying “golden binaries” that could allow for a unique localization [23].

² The current single detector forecasts predict around one strongly lensed event per year per LIGO detector at design sensitivity [11–13].

because the Earth rotates during the delay between image arrivals, each image essentially gives us a new set of detectors with which to localize the event in the sky. A lensed event can thus be localized better in the sky than a non-lensed event (see Fig. 1 for illustration). Indeed, a larger detector network allows for better sky localization [10, 24].

There are approximately 140 lenses per square degree [14]. Once a lensed event has been localized in the sky, additional constraints from the observed image properties should allow us to exclude many of these lenses. When gravitational lensing produces multiple images, typically either two or four bright images form (although in rare scenarios, more images are possible [25–27]). We thus expect that strongly lensed GWs to form two or four images.

The multiple images of the wave travel on different paths through the Universe. The time delay between images is a combination of the difference in path length and in gravitational time dilation from traveling through different parts of the gravitational lens potential well [28]. The characteristic time delay is seconds to months [29–33], depending on the mass of the lens and the alignment of the lens and the source on the sky.

In the case of doubly imaged GWs, there are two pieces of information immediately accessible to us from the GWs: the time delay between the images and the flux ratio of the images. However, these two pieces of information alone will not significantly constrain the lensing system as the time delay is degenerate with the lens mass distribution, and the alignment on the sky. Indeed, many of the lenses within the sky localization area will be consistent with a single time delay and magnification ratio³.

Therefore, we limit our investigation to quadruple image systems. These systems have three independent time delay and magnification ratios: any lens system that cannot produce consistent time delays and magnification ratios cannot be the host of the lensed GW. Indeed, by combining the GW information with the information from the EM side, we can investigate if observations of a quadruply lensed GW event can provide a sufficiently unique fingerprint to definitively identify its host galaxy without an EM counterpart to the GW event.

Let us therefore make the following four assumptions:

1. We detect a quadruply imaged GW event.
2. GW events originate within galaxies that emit EM radiation.

³ Although only massive cluster lenses can produce time delays of order years. The rarity of such clusters might mean that a pair of images with long time delay *is* identifiable to a specific cluster lens, as investigated in Refs. [31, 32, 34]

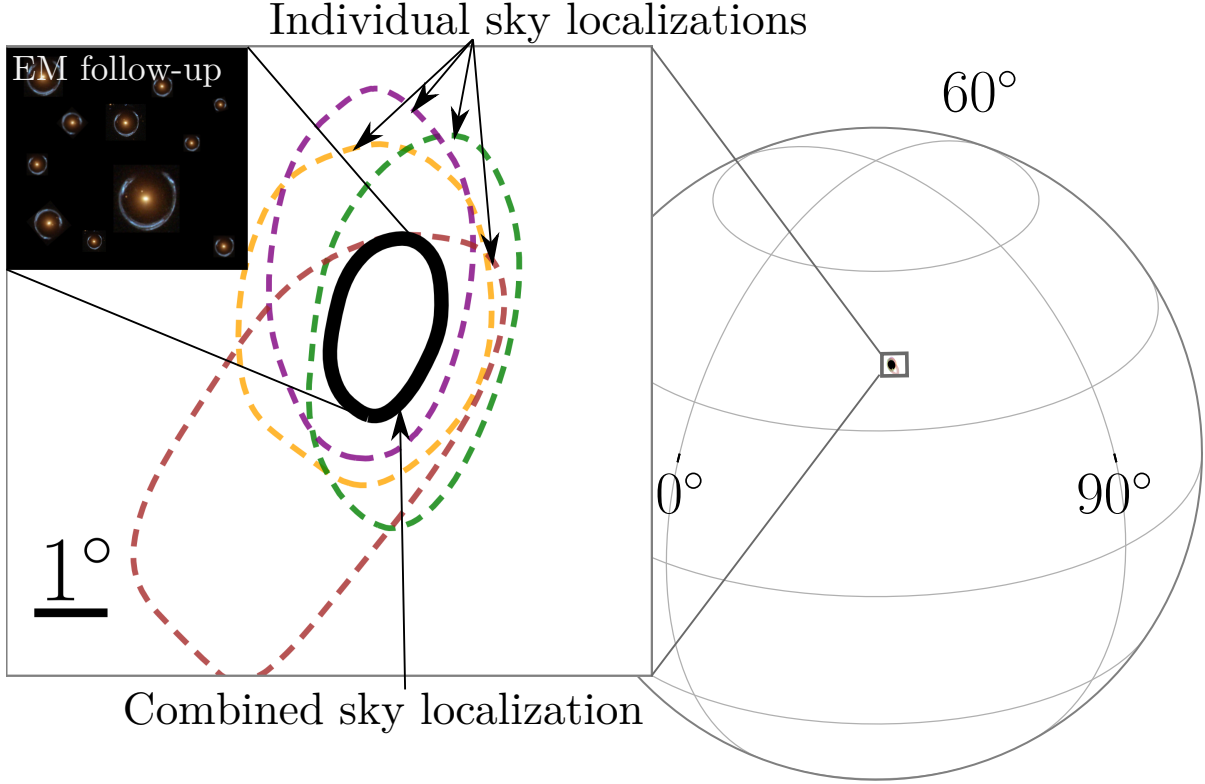


FIG. 1. An illustration of a sky localization of a quadruply lensed gravitational wave. We show both the individual (color) and the combined (black) sky localizations at 90% confidence. Each lensed gravitational-wave essentially gives us a new set of detectors with which to localize the event in sky, allowing for improved sky localization. A dedicated follow-up of the narrowed sky region would then allow us to search for the lensed host galaxy from which the gravitational-wave originates.

3. We identify all of the strong lensing systems within the sky localization of the event.
4. We have redshift information of each lens and source from EM observations.

The first assumption is plausible when LIGO/Virgo reach design sensitivity: Single detector forecasts suggest ~ 1 strongly lensed event per year at LIGO design sensitivity [11–13]. Moreover, Ref. [11] found that $\sim 30\%$ of the detectable lensed events within LIGO would be quadruply lensed. In the third-generation detectors such as the Einstein Telescope [35], we could observe hundreds of lensed events [36, 37]. These estimates assume that the signals that are below the noise threshold can not be detected. However, in the future, there exists an exciting possibility of identifying even some of the signals that are below the noise threshold [38, 39].

The second assumption should apply when the progenitors of binary black holes are stellar

objects. BBH progenitors should trace the star formation rate or the stellar-mass, depending on the delay between massive black hole formation and BBH merger. That the host galaxies emit EM radiation is widely applied in cosmography studies utilizing galaxy catalog based methods [18–22].

The assumption that we know all of the lenses is challenging, even though we expect Euclid and LSST to find $\sim 10^5$ lenses [14]. Euclid lacks the depth to find every faint lensed source, and LSST lacks the angular resolution to detect small Einstein radius systems. However, there is no need to know the strong lenses at the moment the GW event is detected. If the sky localization is restricted to a few square degrees, then dedicated followup of this area with a wide field imaging space telescope like Euclid or WFIRST should quickly go deep enough to detect virtually all of the strongly lensed light (and hence stellar mass) originating at the typical redshifts of lensed GW events [40].

Once the lenses are known, spectroscopic follow-up with a multi-object spectrograph (e.g., 4MOST, DESI, or Mauna Kea Spectroscopic Explorer) could be used to obtain redshifts for the lenses and sources. These facilities have thousands of spectroscopic fibers and fields-of-view of a few square degrees; hence they could simultaneously obtain all of the required redshifts in one or two very deep exposures.

I. THE CATALOG OF STRONGLY LENSED BINARY BLACK HOLE EVENTS

Our simulated lens distribution follows the galaxy-galaxy lens population of Ref. [14]. The lenses are singular isothermal ellipsoid mass profiles with ellipticities and velocity dispersions following the observed distribution from SDSS [41]. We assume these potential lenses are uniformly distributed in a comoving volume out to $z = 2$. Sources are then drawn from the Millennium Simulation [42] with galaxies painted on using a semi-analytic model [43] and matched to the redshift distributions from the Hubble Ultra Deep Field [44]. If the center of the source is multiply imaged, we include the system in our strong lens catalog. This catalog is complete down to sources with an i -band magnitude of 27.

Our lensed GW population follows the lensed galaxy distribution: we treat every lensed source as equally likely to contain a lensed GW event (a more optimal method would involve luminosity and redshift weighting, but we leave this to future work). For the GW properties, we use a power-law black hole mass profile $p(m_1) \propto m^{-2.35}$ with a stellar-mass cut-off at $50 M_\odot$ and uniform in

mass ratio q , consistent with the LIGO/Virgo O1/O2 binary black hole population [45]. We use the IMRPHENOMPv2 waveform model [46–48], which includes the full inspiral, ringdown, and merger parts of the GW signal, as implemented in the LALSUITE software package [49]. We infer the GW parameters using the BILBY parameter inference software [50].

A two or three detector network may have typical sky localization errors larger than we require here, and so we consider four gravitational-wave instruments. We assume the LIGO/Virgo/Kagra network at design sensitivity [51–56], randomly simulate GWs that are quadruply lensed, and choose those that are detectable (i.e., all have a network signal-to-noise ratio $\rho_{\text{network}} > 10$).

II. SKY LOCALIZATION OF MULTIPLY IMAGED EVENTS

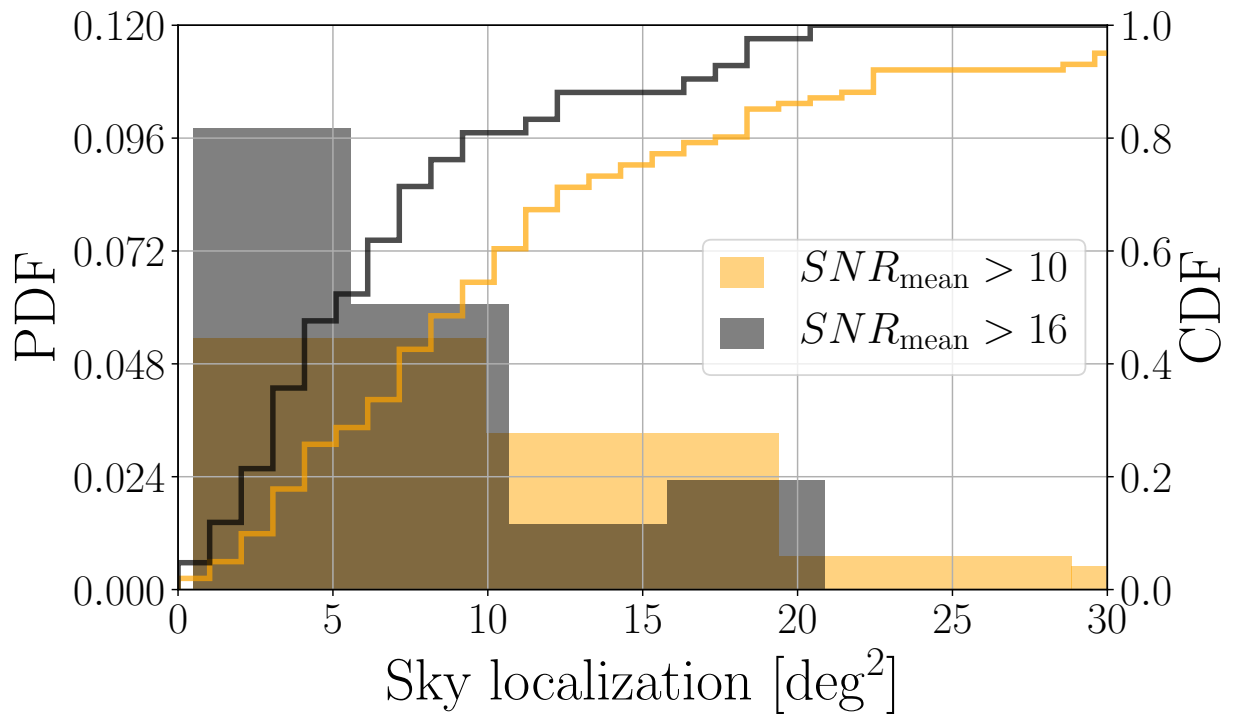


FIG. 2. The probability (histogram) and cumulative distribution function (lines) of the combined sky localization constraints for our catalog of quadruply lensed events in the low (orange) and moderate (black) mean signal-to-noise ratio regimes. We have combined the sky localization posteriors of the four individual lensed events. At both low and moderate signal-to-noise ratio, a large fraction of the events are constrained to better than 10 deg^2 in the sky, and often to better than 5 deg^2 . We quote the 90% confidence interval for the sky localization.

We combine the sky localization posteriors of each image of the quadruply lensed GWs in our simulated catalog, finding that the typical sky localization of moderate (low) signal-to-noise ratio (SNR) detections is $< 10 \text{ deg}^2$ ($< 20 \text{ deg}^2$), and often a much lower $< 5 \text{ deg}^2$ ($< 10 \text{ deg}^2$); see Fig. 2. Since we expect around ~ 140 lens galaxy candidates per square degree [14], quadruple image systems are immediately localized to $\sim \mathcal{O}(100) - \mathcal{O}(1000)$ host systems.

III. IDENTIFYING THE LENS AND SOURCE

Once the event is localized, we can then ask the question ‘which of the observed lenses can reproduce the observed time delays and magnifications?’ Due to the computational costs of inverting the lens equation, we will not be able to perform our full search on a large statistical sample of detected GW injections. Instead, we choose three ‘representative’ injections lensed by large (Einstein radius of $\sim 2 \text{ arcsec}$), medium ($\sim 1 \text{ arcsec}$) and small ($\sim 0.5 \text{ arcsec}$) lens. The simulated binary/lens systems are given in Tables I and II. There are fewer massive lens systems, and they typically produce longer time delays. Thus, we expect that GW events with longer time delays are easier to identify. Lower mass lenses are forecast to be more numerous [14], so we expect that they will be harder to discriminate from each other.

Within the sky localization of each event, we perform lens reconstruction of each possible lens to reproduce the observed time delays and magnification ratios. We model each lens as a singular power-law ellipsoidal mass distribution with external shear. The GW image positions are unknown, but we assume that we already know the lens model parameters to comparable precision to a rough initial lens model obtainable from ground-based imaging of the lensed EM host [57]. Specifically, we assume (0.01, 0.05, 0.03) spread (one-standard-deviation) on the measurement of the Einstein radius, axis-ratio, and each shear component, respectively. We assume the power-law density profile of the lens to be unconstrained by the existing data, adopting instead a prior typical of the strong lens population: a mean slope $\gamma = 2$ with 0.2 spread. These uncertainties are significantly broader than the errors achieved for detailed models of lenses with high-resolution imaging (e.g., Ref. [58–60]). The errors also do not include the correlations between parameters whose inclusion would improve our discriminatory power and are thus conservative. To do the lens inversion, we use LENSTRONOMY, a multi-purpose gravitational lens modeling software package [61]. In the modeling we neglect GW event timing uncertainty, but we add a 20 percent uncertainty on each image magnification to account for lensing by dark substructures.

We compute the Bayes factor for each lens within a sky localization of 4 deg^2 of the GW. Bayes factors are significant for lenses that can reproduce the observed lensed GW events, and low for lenses that are inconsistent with producing the observations. For detailed derivation, see the Methods section.

In our simulation, we find that the Bayes factor allow us to identify the host galaxy when the lens is massive enough (Fig. 3, top panel, orange bins). For smaller lenses, we could narrow down the number of host galaxies to a few or a dozen (Fig. 3, middle and bottom panels, orange bins). We can discriminate larger lenses more easily because they are rare, thus providing characteristic time-delay measurements that are produced by only a few similarly massive lenses.

Systems with a few remaining candidates can be further narrowed down using detailed lens modeling. Therefore, based on the initial ground-based imaging results, we choose the 11 highest Bayes factor candidates⁴ and model high-resolution imaging of each system. Specifically, we use LENSTRONOMY to reconstruct the lens properties observed with a simulated Hubble Space Telescope image. We then find that we can narrow down the lenses to one, four, and five for the large, medium, and small lens scenarios, respectively (Fig. 3, black bins).

Therefore, we can generally localize the GW source to one or at most a few galaxies. The number of potential host galaxy candidates scales with the sky area. Thus, moderate to high signal-to-noise ratio detections will be more promising and will allow us to discriminate the sources better. We expect more precise modeling of the lens and GW priors, and the inclusion of so-called joint-PE methodologies [63] to also improve our discriminatory power.

⁴ This could be the default analysis if automatic lens modeling [62] can produce high fidelity lens models for every strong lens within the sky localization.

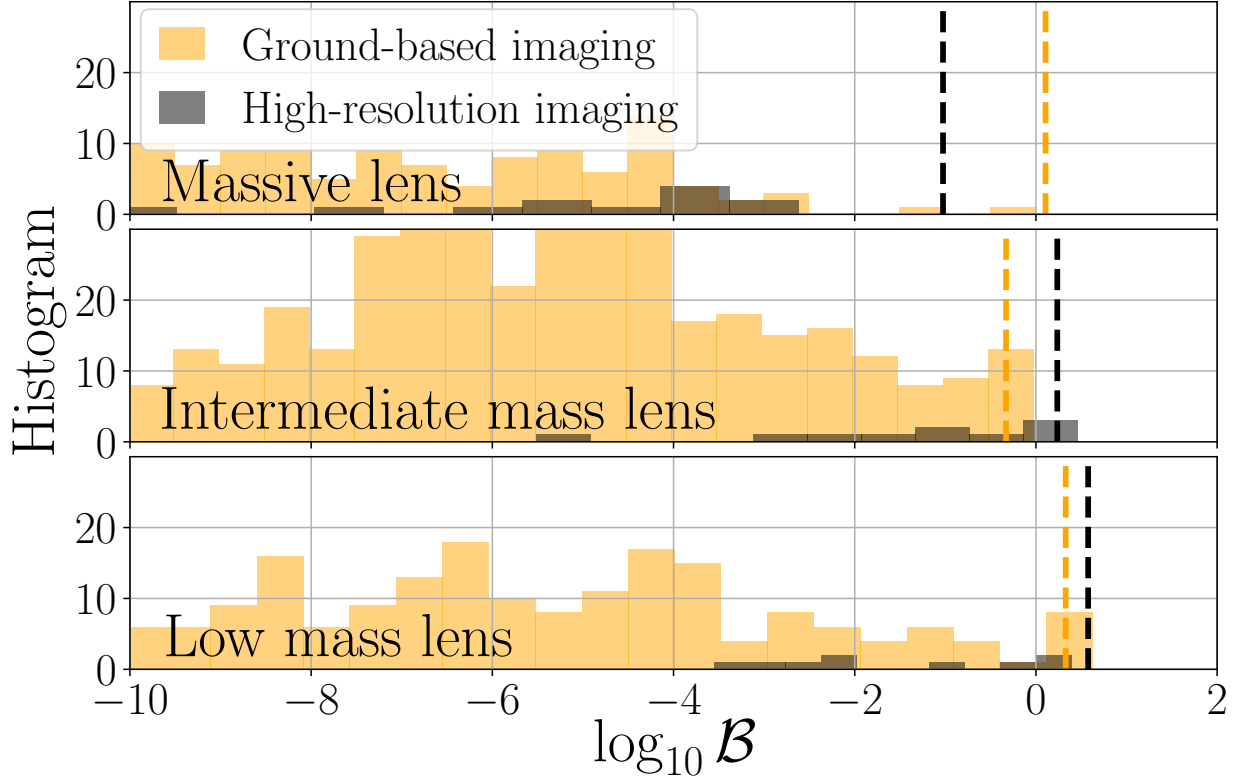


FIG. 3. The Bayes factor in favor of a given galaxy being the host of the merging black hole. We show the results for 550 lens reconstructions within the sky localization of the injected gravitational-wave using ground-based imaging (orange). The Bayes factor for the 11 best fitting lenses are shown in black after modeling simulated high-resolution follow up imaging. The Bayes factors are large for lenses that can reproduce the observed lensed GW event properties, and low for lenses that are inconsistent with producing the observations. We show three lensing configurations: a gravitational-wave lensed by a massive ~ 2 arcsec Einstein radius lens (top panel), a moderate ~ 1 arcsec lens (middle panel), and a small ~ 0.5 arcsec lens (bottom panel). The correct lens yields a high Bayes factor in all three cases (vertical dashed lines). In the massive lens scenario (top panel), the background of lensed galaxy candidates is separated. Thus, we can uniquely narrow down the source to one galaxy at above 90% confidence with high-resolution imaging. In the moderate and small lens scenarios (middle and bottom panels), we narrow down the host galaxy to four and five candidates, respectively.

IV. LOCATING THE BBH MERGER WITHIN THE LENSED HOST AND MEASURING THE HUBBLE CONSTANT

Once the GW host system has been identified, a detailed lens model can be used to de-lens the EM source, identify which positions on the source plane can produce the observed time-delays and magnifications, and to convert time-delays and magnifications into inference on the Hubble constant. We use LENSTRONOMY to reconstruct a typical Einstein ring observed with a simulated Hubble Space Telescope image, shown in Fig. 4.

We simulate random realizations of lensed GWs in this system until one of them is detected as a quadruple image event within LIGO/Virgo/Kagra. Given the lens model, the time delay ratios and magnification ratios localize the lens within the source. However, the symmetry of the lensing system means the source position is not uniquely determined. Marginalizing over the uncertainty in the lens and source parameters enables us to locate the BBH merger to one of two regions ⁵.

Since the ratio of time delays and magnifications is sufficient to constrain the source position, the absolute scale of the time delays and the absolute magnifications are still sensitive to the Hubble constant even without an EM counterpart. The time delays are sensitive to the Hubble constant through the time delay distance [28, 64], and the magnifications are sensitive through the luminosity distance to the GW source because BBHs can be regarded as standard sirens [2, 65]. Converting the distances to cosmological parameter inference requires knowledge of lens and source redshifts, but these can be measured in the EM.

To illustrate the cosmological sensitivity, we show constraints on the Hubble constant, in a flat Λ CDM cosmology with Ω_M fixed. We show the inferred H_0 in Fig. 5. Combining the H_0 constraints from the time delay distance and the four images of the standard siren, we find $H_0 = 68^{+8}_{-6} \text{ km s}^{-1} \text{ Mpc}^{-1}$ (median with symmetric 68% credible interval).

⁵ The lens model localizes the source position to one of four regions, but these are blurred into two distinct regions after combining with the uncertainty on the source position inferred from the EM modeling

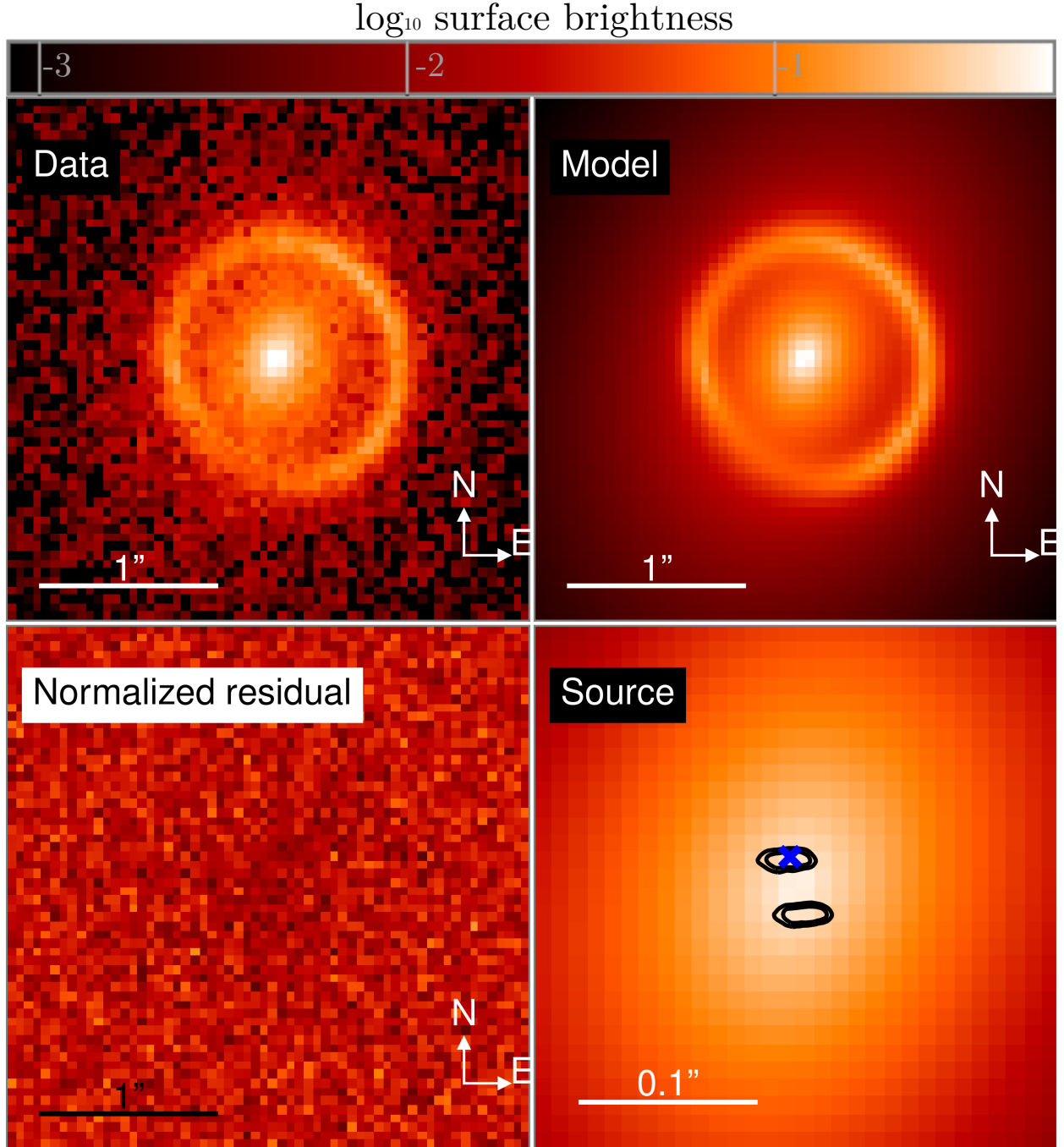


FIG. 4. The sample lens system we use in our simulated Hubble constant measurement. Top-left panel: Observed light distribution. Top-right panel: Best fit model of the lens and the source. Bottom-left panel: The difference after subtracting the model from the data. Bottom-right panel: The reconstruction of the unlensed source for the best fitting model, and the inferred position of the binary black hole relative to the source at 90% confidence (black contour) as well as its true position (blue cross).

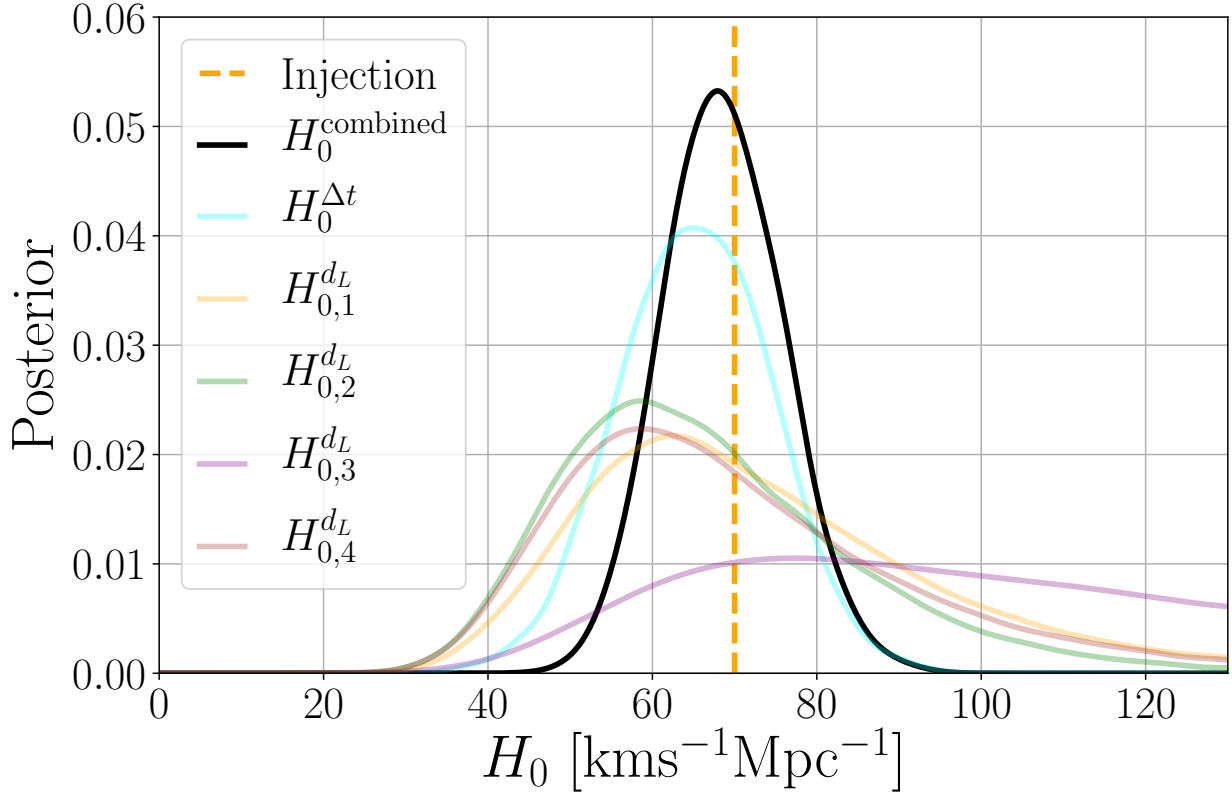


FIG. 5. Measurement of the Hubble constant H_0 from the combination of gravitational-wave data and the lensed EM host galaxy (black). The coloured lines show the H_0 inferred from each of the four lensed gravitational wave ‘standard siren’ posteriors and the time-delay distance measurement (cyan). Combining these constraints yields a more stringent H_0 measurement compared to the individual posteriors. The dashed line shows the simulated value of $H_0 = 70 \text{ kms}^{-1} \text{Mpc}^{-1}$.

The primary contribution to the H_0 measurement comes from the measurement of the time-delay distance. The secondary contribution is from the standard siren. However, the latter is predicated on a 20 percent uncertainty for the magnification of the GW images. This is significantly smaller than expected for lensed supernovae [66], where stellar microlensing plays a significant role. However, microlensing is not expected to be as significant for lensed GWs as the Einstein radius of a star is smaller than the wavelength of stellar-mass BBH gravitational wave emission [67] (except in the case of extreme macro model magnification [68]). A dedicated study towards gravitational-wave microlensing will be needed to quantify a more realistic estimate of the magnification uncertainties due to microlensing. Such a study will require detailed wave optics modeling [69] and is beyond the scope of this work.

For the Hubble constant inference, we have individually modeled each of the magnified standard sirens despite them being images of the same event, a joint-PE based parameter estimation could remove these excess degrees of freedom and improve the H_0 constraint [63].

V. DISCUSSION AND CONCLUSION

We have presented a method that can uniquely localize the host galaxies of gravitational waves from *binary black holes* using quadruply lensed gravitational waves. Localizing the host galaxy could enable several scientific frontiers. We could measure the redshift of the galaxy and thus binary, allowing us to measure the Hubble constant and perform cosmography studies, as we have shown here. Moreover, by obtaining the source galaxy redshift and position in the sky, we might perform accurate tests of GW propagation and improved polarization tests with effectively more detectors [34, 70]. We could also study the interconnection between host galaxies and the massive black hole population discovered within LIGO/Virgo [45, 71].

In some scenarios, we will only be able to localize the source host galaxy to a few candidates. These systems can still contribute to statistical studies. For example, we can perform cosmography studies by marginalizing the Hubble constant measurement according to the Bayes factor of each candidate. Comparable methods have been developed for Hubble constant measurements utilizing galaxy catalogs [18–22].

With the recently approved A+ detector upgrade [72], the sky localization should further improve. As the sky localization improves, lens identification becomes proportionately easier. In the third-generation detectors such as the Einstein Telescope [35], we could observe hundreds of lensed events at even higher signal-to-noise ratio [36, 37]. In the era of future detectors identifying the hosts of quadruply imaged GWs should regularly be possible without an EM counterpart.

VI. ACKNOWLEDGEMENTS

We thank David Keitel, Ken Ng, Ignacio Magana Hernandez, Chris van den Broeck, Archisman Ghosh, Daniel Holz, Peter Pang, Rico Lo, and Ian Harry for discussions, comments and feedback. OAH is supported by the research program of the Netherlands Organization for Scientific Research (NWO). TEC is funded by a Royal Astronomical Society Research Fellowship and by a Dennis Sciama Fellowship from the University of Portsmouth. MÇ is supported by the Enrico Fermi

Institute. TGFL is partially supported by grants from the Research Grants Council of the Hong Kong (Project No. 14306218), Research Committee of the Chinese University of Hong Kong and the Croucher Foundation of Hong Kong. The sky map in Fig. 1 uses the LIGO.SKYMAP package and the lens image is a modified version of a Hubble Space Telescope image of the Cosmic Horseshoe. The authors are grateful for computational resources provided by the LIGO Laboratory and supported by National Science Foundation Grants PHY-0757058 and PHY-0823459.

Appendix A: Methodology

1. Determination of the Hubble constant from angular diameter distances

For any given lens system, the Hubble constant is related to the time-delays measured from the GWs by [64]

$$\Delta t_{ij} = \frac{D_{\Delta t}(z, z_L, H_0^{\Delta t})(1 + z_L)}{c} \Delta \phi_{ij}, \quad (\text{A1})$$

where z_s and z_L are the source and lens redshifts, $\Delta \phi_{ij}$ is the reconstructed fermat potential at the image positions (for i, j pairs of images), Δt_{ij} is the lensing time-delay between the two GW signals, and

$$D_{\Delta t}(z, z_L, H_0^{\Delta t}) = \frac{d_A(z_L, H_0^{\Delta t})d_A(z_s, H_0^{\Delta t})}{d_A(z_L, z_s, H_0^{\Delta t})}, \quad (\text{A2})$$

is a combination of the angular diameter distances.

We can retrieve the fermat potential between the two images $\Delta \phi_{ij}$ and $D_{\Delta t}$ in *unison* by solving the lens equation for a quad system. In particular, the lens system will have four source positions and unique time-delay distance for a given combination of GW time-delays $\{t_i\}$. After solving the time-delay distance $D_{\Delta t}$, we can retrieve H_0 from Eq. A2. Its posterior distribution

$$\begin{aligned} p(H_0^{\Delta t} | d_{\text{EM}}^t) &= p(H_0^{\Delta t} | \vec{\theta}_L, z_L, z_s, \{t_i\}) \\ &= p(\vec{\theta}_L, z_L, z_s, \{t_i\} | d_{\text{EM}}^t), \end{aligned} \quad (\text{A3})$$

where d_{EM}^t includes the EM data (lens reconstruction, redshift measurements) and the GW time-delay data. The posterior $p(\vec{\theta}_L, z_L, z_s, \{t_i\} | d_{\text{EM}}^t)$ includes the lens parameters $\vec{\theta}_L$, the redshifts (z_L, z_s) , and the GW time-delays $\{t_i\}$.

2. Determination of the magnification and luminosity distance from GWs

We can alternatively measure the Hubble constant by using the absolute image magnifications. To do so, we first need to match the relative magnification of the GW observations with those obtained from the lens reconstruction.

The GW measurement of the luminosity distance is fully degenerate with the magnification of the signal, i.e.,

$$D_{\text{obs}}^i = d_L / \sqrt{\mu_i}, \quad (\text{A4})$$

where D_{obs}^i is the observed luminosity distance (as inferred from the GWs) of the i th signal and μ_i is the corresponding magnification. d_L is the true luminosity distance of the object.

Even without the complementary knowledge of the lens system, we can straightforwardly compute the relative magnification

$$\mu_r^{ij} = \frac{\mu_i}{\mu_j} = \left(\frac{D_{\text{obs}}^j}{D_{\text{obs}}^i} \right)^2. \quad (\text{A5})$$

which is the division of the two *observed* luminosity distance posteriors. The posterior (taking the dominant correlation between parameters to be between the inclination and luminosity distance)

$$\begin{aligned} p(\mu_r^{ij} | d_{\text{GW}}) &\approx \int p(\mu_r^{ij} | D_{\text{obs}}^i, D_{\text{obs}}^j) \\ &\times \left(\frac{p(D_{\text{obs}}^i, \iota | d_i) p(D_{\text{obs}}^j, \iota | d_j)}{p(D_{\text{obs}}^i | d_i) p(D_{\text{obs}}^j | d_j) p(D_{\text{obs}}^j) p(\iota)^2} \right) \\ &\times p(\iota) p(D_{\text{obs}}^i | d_i) p(D_{\text{obs}}^j | d_j) dD_{\text{obs}}^i dD_{\text{obs}}^j d\iota, \end{aligned} \quad (\text{A6})$$

where ι is the inclination, which we included because it is highly degenerate with luminosity distance⁶, and we assume a flat (agnostic) μ_{rel} prior. The $d_{\text{GW}} = \{d_i\}$ is the GW data strains, and d_i is the i th observed GW strain. Note that in the lensing hypothesis all the parameters of the four signals will be the same, except for the observed luminosity-distance, time of coalescence, and phase of coalescence [29]. Here we have assumed that the dominant correlation between luminosity distance and other parameters is the inclination, which is supported by several analyses detailing the luminosity distance-inclination degeneracy (e.g. [73, 74]). Nevertheless, including all correlations could slightly improve our measurement accuracies.

3. Determination of the lensing magnifications

Given the lens model and the time-delays $\{t_i\}$, we obtain four potential source positions $\{\vec{y}^k\}$ with $k = 0, 1, 2, 3$ being the source position index (i.e., we obtain four source positions, each of which will have four corresponding image positions). For each source position, we retrieve four lensing magnifications $\{\mu_i^k\}$, where i is the image index and k the source index. The posterior distribution

$$\begin{aligned} p(\{\mu_i^k\} | d_{\text{EM}}^t) &= p(\{\mu_i^k\} | \vec{\theta}_L, z_L, z_s, \{t_i\}) \\ &p(\vec{\theta}_L, z_L, z_s, \{t_i\} | d_{\text{EM}}^t) d\vec{\theta}_L dz_L dz_s d\{t_i\}. \end{aligned} \quad (\text{A7})$$

⁶ If inclination was excluded, the relative magnification μ_r would be poorly constrained.

The GWs give us the *relative* magnifications $\mu_r^{ij} = \mu_i/\mu_j$ at a moderate accuracy. We can use this to test if the GW comes from this specific lensing system as follows: Let the lensed and the null hypothesis be

$$\begin{aligned}\mathcal{H}_\mu : \mu_r^{ij} + \delta\mu_r^{ij} &= \tilde{\mu}_r^{ij} = \mu_r^{ijk} = \frac{\mu_i^k}{\mu_j^k} \text{ for some } k, \\ \mathcal{H}_0 : \mu_r^{ij} \text{ and } \mu_r^{ijk} &= \frac{\mu_i^k}{\mu_j^k} \text{ are independent for all } k,\end{aligned}\tag{A8}$$

where $\delta\mu_r^{ij}$ introduces a 20% error spread due to weak and microlensing. However, we note that microlensing can be suppressed for GWs due to *diffraction* effects in the case of stellar-mass microlenses [67] (except in the case of extreme macromodel magnification [68]). A dedicated study towards gravitational-wave microlensing will be needed to quantify a more realistic estimate of the magnification uncertainties due to microlensing. Such a study will require detailed wave optics modeling [69] and is thus outside the scope of this work.

The Bayes factor between the two hypotheses is then

$$\begin{aligned}\mathcal{M}_0^\mu &\approx \frac{1}{4} \sum_k \int \prod_{ij} p(\tilde{\mu}_r^{ij} | d_{\text{GW}}, \mathcal{H}_0) p(\mu_r^{ij} | d_{\text{EM}}^t, \mathcal{H}_0, k) \\ &\quad p(\mu_r^{ij} | \mathcal{H}_0)^{-1} d\mu_r^{ij},\end{aligned}\tag{A9}$$

where $p(\tilde{\mu}_r^{ij} | d_{\text{GW}}, \mathcal{H}_0)$ is the relative magnification from the GW luminosity distances only, marginalized over the microlensing error, $p(\mu_r^{ij} | d_{\text{EM}}^t, \mathcal{H}_0, k)$ is the relative magnification predicted from the time-delay and the reconstructed lens for the source index k , and $p(\mu_r^{ij} | \mathcal{H}_0)$ is the relative magnification prior. The integral can be solved by importance sampling of the $p(\mu_r^{ij} | d_{\text{EM}}^t, \mathcal{H}_0, k)$. We assume that the relative magnification prior is uniform; this assumption is roughly consistent with the findings in Ref. [13]. Future studies are expected to assign more accurate priors as they become available. We stress that this will allow for a more *optimal* definition of the Bayes factor but is not expected to hinder our analysis.

The correct source index k is the one for which there is the largest evidence

$$\begin{aligned}\frac{p(d | \mathcal{H}_\mu, k)}{p(d | \mathcal{H}_0)} &= \prod_{ij} \int p(\tilde{\mu}_r^{ij} | \mathcal{H}_0, d_{\text{GW}}) p(\mu_r^{ij} | d_{\text{EM}}^t, \mathcal{H}_0, k) \\ &\quad p(\mu_r^{ij} | \mathcal{H}_0)^{-1} d\mu_r^{ij},\end{aligned}\tag{A10}$$

where (i, j) run through $(0, 1), (1, 2), (2, 3)$. We thus weight each sample by the evidence for the given source index. In principle, if the evidence for a given source index $k = k_0$ is substantial, we

could retrieve the correct magnification posteriors

$$p(\{\mu_i\}|d_{\text{EM}}^t) = p(\{\mu_i\}|\vec{\theta}_L, z_L, z_s, \{t_i\})p(\vec{\theta}_L, z_L, z_s, \{t_i\}|d_{\text{EM}}^t), \quad (\text{A11})$$

where we have removed the index k and assumed it to be $k = k_0$ to simplify the notation. However, note that we do not choose a specific source index in our analysis, or the one with the most substantial evidence. Instead, we (correctly) weigh each source index according to the evidence (Eq. A10).

4. Determination of the Hubble constant from luminosity distance

After retrieving the image magnifications, we can estimate the Hubble constant a secondary way, using the host galaxy redshift z_s

$$d_L(z_s, H_{0,i}^{d_L}) = \frac{(1 + z_s)c}{H_{0,i}^{d_L}} F(z_s). \quad (\text{A12})$$

This allows us to measure the Hubble constant whose posterior

$$\begin{aligned} p(H_{0,i}^{d_L}|d_{\text{GW}}, d_{\text{EM}}^t) &= \int p(H_{0,i}^{d_L}|z_s, d_L)p(z_s|d_{\text{EM}}) \\ &\quad p(d_L|d_{\text{GW}}, \mu_i) \\ &\quad p(\mu_i|d_{\text{EM}}^t) dz_s dd_L d\mu_i, \end{aligned} \quad (\text{A13})$$

where we mark the i th image and the corresponding Hubble constant measurement $H_{0,i}^{d_L}$ with index i .

5. Identifying the lens galaxy based on Hubble constant measurements

Once we have measured the Hubble constants $H_0^{\{\Delta t, d_L\}}$, we can perform two additional tests to identify the correct lensed host galaxy. The Hubble constant $H_0^{\Delta t}$ must be within its expected prior range

$$\mathcal{R}_0^\mu = \int \frac{p(H_0^{\Delta t}|d_{\text{EM}}^t)p(H_0^{\Delta t}|\mathcal{H}'_\mu)}{p(H_0^{\Delta t}|\mathcal{H}'_0)} dH_0^{\Delta t}, \quad (\text{A14})$$

where $p(H_0^{\Delta t}|\mathcal{H}'_\mu) \in [60, 80] \text{ km s}^{-1} \text{ Mpc}^{-1}$ is the expected prior range, and $p(H_0^{\Delta t}|\mathcal{H}'_0)$ is some much wider prior range corresponding to the case that the galaxy is not the host. Here we choose the wider prior to be $H_0^{\Delta t} \in [0, 1000] \text{ km s}^{-1} \text{ Mpc}^{-1}$. In principle, we can retrieve a more accurate

prior choice for $H_0^{\Delta t}$ by sampling the expected lens distribution. Doing so would likely improve our discriminatory power.

Likewise, the secondary Hubble constant measurement $H_{0,i}^{d_L}$ must be within the expected prior

$$\tilde{\mathcal{R}}_0^\mu = \prod_i \int \frac{p(H_{0,i}^{d_L} | d_{\text{GW}}, d_{\text{EM}}^t) p(H_{0,i}^{d_L} | \mathcal{H}'_\mu)}{p(H_{0,i}^{d_L} | \mathcal{H}'_0)} dH_{0,i}^{d_L}. \quad (\text{A15})$$

Therefore, the total log Bayes factor for/against the hypothesis that the GW originates from a given lens candidate is

$$\log \mathcal{B}_0^\mu = \log \mathcal{M}_0^\mu + \log \mathcal{R}_0^\mu + \log \tilde{\mathcal{R}}_0^\mu. \quad (\text{A16})$$

6. Combined sky localization of a lensed wave

Given that we have detected a quadruply lensed gravitational wave, we can combine their sky localization posteriors simply by re-weighting:

$$p(\text{ra}, \text{dec} | d_1, d_2, d_3, d_4) \propto \frac{\prod_{i=1}^4 p(\text{ra}, \text{dec} | d_i)}{p(\text{ra}, \text{dec})^3}, \quad (\text{A17})$$

where we neglect the correlations between the other gravitational-wave parameters and the sky localization, as well as selection effects. Their inclusion would improve our ability to localize the event in the sky.

Injection	m_1	m_2	z_L	z_s	θ_E	q	γ	γ_1	γ_2
1	9 M_\odot	7 M_\odot	0.17	0.97	2"	0.9	2.1	0.04	0.03
2	11 M_\odot	10 M_\odot	0.16	0.94	1"	0.8	1.8	0	-0.02
3	7 M_\odot	5 M_\odot	0.99	1.60	0.5"	0.7	1.7	-0.01	0.08

TABLE I. The binary masses m_1, m_2 , the lens and source redshifts z_L and z_s , Einstein radius θ_E , axis ratio q , power-law slope γ and the shears γ_1 and γ_2 of our simulated lensed signals.

-
- [1] B. P. Abbott et al. GW170817: Observation of Gravitational Waves from a Binary Neutron Star Inspiral. *Phys. Rev. Lett.*, 119(16):161101, 2017.
 - [2] B. P. Abbott et al. A gravitational-wave standard siren measurement of the Hubble constant. *Nature*, 551(7678):85–88, 2017.

Injection	Δt^{12}	Δt^{23}	Δt^{34}	μ_1	μ_2	μ_3	μ_4
1	7.2 days	18.1 days	14.0 days	6.3	7.1	6.7	5.0
2	4.6 days	3.3 hours	4.4 hours	5.0	20.2	12.9	9.6
3	2.4 days	4.0 days	1.7 days	3.6	4.2	2.6	2.0

TABLE II. Relative time-delays between signals t^{ij} and the image magnifications $\{\mu_i\}$ for our simulated lensed signals.

- [3] Emanuele Berti et al. Testing General Relativity with Present and Future Astrophysical Observations. *Class. Quant. Grav.*, 32:243001, 2015.
- [4] Juan Calderón Bustillo, Pablo Laguna, and Deirdre Shoemaker. Detectability of gravitational waves from binary black holes: Impact of precession and higher modes. *Phys. Rev.*, D95(10):104038, 2017.
- [5] Peter T. H. Pang, Juan Calderón Bustillo, Yifan Wang, and Tjonnie G. F. Li. Potential observations of false deviations from general relativity in gravitational wave signals from binary black holes. *Phys. Rev.*, D98(2):024019, 2018.
- [6] Katerina Chatziioannou et al. On the properties of the massive binary black hole merger GW170729. *Phys. Rev.*, D100(10):104015, 2019.
- [7] B.P. Abbott et al. Tests of General Relativity with the Binary Black Hole Signals from the LIGO-Virgo Catalog GWTC-1. *Phys. Rev. D*, 100(10):104036, 2019.
- [8] M. Coleman Miller and Nicolás Yunes. The new frontier of gravitational waves. *Nature*, 568(7753):469–476, 2019.
- [9] GW190412: Observation of a Binary-Black-Hole Coalescence with Asymmetric Masses. 4 2020.
- [10] B.P. Abbott et al. Prospects for Observing and Localizing Gravitational-Wave Transients with Advanced LIGO, Advanced Virgo and KAGRA. *Living Rev. Rel.*, 21(1):3, 2018.
- [11] Shun-Sheng Li, Shude Mao, Yuetong Zhao, and Youjun Lu. Gravitational lensing of gravitational waves: a statistical perspective. *MNRAS*, 476(2):2220–2229, May 2018.
- [12] Ken K. Y. Ng, Kaze W. K. Wong, Tom Broadhurst, and Tjonnie G. F. Li. Precise ligo lensing rate predictions for binary black holes. *Phys. Rev. D*, 97:023012, Jan 2018.
- [13] Masamune Oguri. Effect of gravitational lensing on the distribution of gravitational waves from distant binary black hole mergers. *MNRAS*, 480(3):3842–3855, Nov 2018.

- [14] Thomas E. Collett. The Population of Galaxy-Galaxy Strong Lenses in Forthcoming Optical Imaging Surveys. *ApJ*, 811(1):20, September 2015.
- [15] LIGO Scientific Collaboration and Virgo Collaboration. https://gcn.gsfc.nasa.gov/lvc_events.html, 2019.
- [16] LIGO Scientific Collaboration and Virgo Collaboration. <https://gracedb.ligo.org/latest/>, 2019.
- [17] B. P. Abbott et al. GWTC-1: A Gravitational-Wave Transient Catalog of Compact Binary Mergers Observed by LIGO and Virgo during the First and Second Observing Runs. *Phys. Rev.*, X9(3):031040, 2019.
- [18] Hsin-Yu Chen, Maya Fishbach, and Daniel E. Holz. A two per cent Hubble constant measurement from standard sirens within five years. *Nature*, 562(7728):545–547, 2018.
- [19] M. Fishbach et al. A Standard Siren Measurement of the Hubble Constant from GW170817 without the Electromagnetic Counterpart. *Astrophys. J.*, 871(1):L13, 2019.
- [20] Rachel Gray et al. Cosmological Inference using Gravitational Wave Standard Sirens: A Mock Data Challenge. 2019.
- [21] B. P. Abbott et al. A gravitational-wave measurement of the Hubble constant following the second observing run of Advanced LIGO and Virgo. 2019.
- [22] M. Soares-Santos et al. First Measurement of the Hubble Constant from a Dark Standard Siren using the Dark Energy Survey Galaxies and the LIGO/Virgo Binary–Black-hole Merger GW170814. *Astrophys. J.*, 876(1):L7, 2019.
- [23] Hsin-Yu Chen and Daniel E. Holz. Finding the One: Identifying the Host Galaxies of Gravitational-Wave Sources. 12 2016.
- [24] B. P. Abbott et al. GW170814: A Three-Detector Observation of Gravitational Waves from a Binary Black Hole Coalescence. *Phys. Rev. Lett.*, 119(14):141101, 2017.
- [25] Thomas E. Collett and David J. Bacon. Compound lensing: Einstein zig-zags and high-multiplicity lensed images. *MNRAS*, 456(2):2210–2220, February 2016.
- [26] H. Dahle et al. SDSSJ2222+2745 A Gravitationally Lensed Sextuple Quasar with Maximum Image Separation of 15.1’ Discovered in the Sloan Giant Arcs Survey. *Astrophys. J.*, 773:146, 2013.
- [27] Thomas E. Collett et al. Core or Cusps: The Central Dark Matter Profile of a Strong Lensing Cluster with a Bright Central Image at Redshift 1. *Astrophys. J.*, 843(2):148, 2017.

- [28] S. Refsdal. On the possibility of determining Hubble’s parameter and the masses of galaxies from the gravitational lens effect. *MNRAS*, 128:307, January 1964.
- [29] K. Haris, A. K. Mehta, S. Kumar, T. Venumadhav, and P. Ajith. Identifying strongly lensed gravitational wave signals from binary black hole mergers. *arXiv e-prints*, July 2018.
- [30] O. A. Hannuksela, K. Haris, K. K. Y. Ng, S. Kumar, A. K. Mehta, D. Keitel, T. G. F. Li, and P. Ajith. Search for gravitational lensing signatures in ligo-virgo binary black hole events. *The Astrophysical Journal*, 874(1):L2, Mar 2019.
- [31] Graham P. Smith, Mathilde Jauzac, John Veitch, Will M. Farr, Richard Massey, and Johan Richard. What if LIGO’s gravitational wave detections are strongly lensed by massive galaxy clusters? *Mon. Not. Roy. Astron. Soc.*, 475(3):3823–3828, 2018.
- [32] Graham P. Smith, Andrew Robertson, Matteo Bianconi, and Mathilde Jauzac. Discovery of strongly-lensed gravitational waves - implications for the lsst observing strategy, 2019.
- [33] Andrew Robertson, Graham P. Smith, Richard Massey, Vincent Eke, Mathilde Jauzac, Matteo Bianconi, and Dan Rychanowski. What does strong gravitational lensing? The mass and redshift distribution of high-magnification lenses. 2020.
- [34] G. P. Smith et al. Strong-lensing of Gravitational Waves by Galaxy Clusters. *IAU Symp.*, 338:98–102, 2017.
- [35] Michele Maggiore et al. Science Case for the Einstein Telescope. 2019.
- [36] Marek Biesiada, Xuheng Ding, Aleksandra Piórkowska, and Zong-Hong Zhu. Strong gravitational lensing of gravitational waves from double compact binaries—perspectives for the Einstein Telescope. *J. Cosmology Astropart. Phys.*, 2014(10):080, Oct 2014.
- [37] Xuheng Ding, Marek Biesiada, and Zong-Hong Zhu. Strongly lensed gravitational waves from intrinsically faint double compact binaries—prediction for the Einstein Telescope. *J. Cosmology Astropart. Phys.*, 2015(12):006, Dec 2015.
- [38] Alvin K. Y. Li, Rico K. L. Lo, Surabhi Sachdev, C. L. Chan, E. T. Lin, Tjonnie G. F. Li, and Alan J. Weinstein. Targeted Sub-threshold Search for Strongly-lensed Gravitational-wave Events. 2019.
- [39] Connor McIsaac, David Keitel, Thomas Collett, Ian Harry, Simone Mozzon, Oliver Edy, and David Bacon. Search for Strongly Lensed Counterpart Images of Binary Black Hole Mergers in the First Two LIGO Observing Runs. 2019.
- [40] Dan Rychanowski. personal communication.

- [41] Yun-Young Choi, Changbom Park, and Michael S. Vogeley. Internal and Collective Properties of Galaxies in the Sloan Digital Sky Survey. *ApJ*, 658(2):884–897, April 2007.
- [42] Volker Springel, Simon D. M. White, Adrian Jenkins, Carlos S. Frenk, Naoki Yoshida, Liang Gao, Julio Navarro, Robert Thacker, Darren Croton, John Helly, John A. Peacock, Shaun Cole, Peter Thomas, Hugh Couchman, August Evrard, Jörg Colberg, and Frazer Pearce. Simulations of the formation, evolution and clustering of galaxies and quasars. *Nature*, 435(7042):629–636, June 2005.
- [43] Gabriella De Lucia and J  r  my Blaizot. The hierarchical formation of the brightest cluster galaxies. *MNRAS*, 375(1):2–14, February 2007.
- [44] A. J. Connolly, John Peterson, J. Garrett Jernigan, Robert Abel, Justin Bankert, Chihway Chang, Charles F. Claver, Robert Gibson, David K. Gilmore, Emily Grace, R. Lynne Jones, Zeljko Ivezic, James Jee, Mario Juric, Steven M. Kahn, Victor L. Krabbendam, Simon Krughoff, Suzanne Lorenz, James Pizagno, Andrew Rasmussen, Nathan Todd, J. Anthony Tyson, and Mallory Young. *Simulating the LSST system*, volume 7738 of *Society of Photo-Optical Instrumentation Engineers (SPIE) Conference Series*, page 77381O. 2010.
- [45] B. P. Abbott et al. Binary Black Hole Population Properties Inferred from the First and Second Observing Runs of Advanced LIGO and Advanced Virgo. *Astrophys. J.*, 882(2):L24, 2019.
- [46] Mark Hannam, Patricia Schmidt, Alejandro Boh  , Le  la Haegel, Sascha Husa, Frank Ohme, Geraint Pratten, and Michael P  rrer. Simple Model of Complete Precessing Black-Hole-Binary Gravitational Waveforms. *Phys. Rev. Lett.*, 113(15):151101, 2014.
- [47] Sascha Husa, Sebastian Khan, Mark Hannam, Michael P  rrer, Frank Ohme, Xisco Jim  nez Forteza, and Alejandro Boh  . Frequency-domain gravitational waves from nonprecessing black-hole binaries. I. New numerical waveforms and anatomy of the signal. *Phys. Rev.*, D93(4):044006, 2016.
- [48] Sebastian Khan, Sascha Husa, Mark Hannam, Frank Ohme, Michael P  rrer, Xisco Jim  nez Forteza, and Alejandro Boh  . Frequency-domain gravitational waves from nonprecessing black-hole binaries. II. A phenomenological model for the advanced detector era. *Phys. Rev.*, D93(4):044007, 2016.
- [49] LIGO Scientific Collaboration. LIGO Algorithm Library - LALSuite. free software (GPL), 2018.
- [50] Gregory Ashton, Moritz H  bner, Paul D. Lasky, Colm Talbot, Kendall Ackley, Sylvia Biscoveanu, Qi Chu, Atul Divakarla, Paul J. Easter, Boris Goncharov, Francisco Hernandez Vivanco, Jan Harms, Marcus E. Lower, Grant D. Meadors, Denyz Melchor, Ethan Payne, Matthew D. Pitkin, Jade Powell, Nikhil Sarin, Rory J. E. Smith, and Eric Thrane. BILBY: A User-friendly Bayesian Inference Library for Gravitational-wave Astronomy. *ApJS*, 241(2):27, Apr 2019.

- [51] J. Aasi et al. Advanced LIGO. *Class. Quant. Grav.*, 32:074001, 2015.
- [52] B. P. Abbott et al. GW150914: The Advanced LIGO Detectors in the Era of First Discoveries. *Phys. Rev. Lett.*, 116(13):131103, 2016.
- [53] F. Acernese et al. Advanced Virgo: a second-generation interferometric gravitational wave detector. *Class. Quant. Grav.*, 32(2):024001, 2015.
- [54] Kentaro Somiya. Detector configuration of KAGRA: The Japanese cryogenic gravitational-wave detector. *Class. Quant. Grav.*, 29:124007, 2012.
- [55] Yoichi Aso, Yuta Michimura, Kentaro Somiya, Masaki Ando, Osamu Miyakawa, Takanori Sekiguchi, Daisuke Tatsumi, and Hiroaki Yamamoto. Interferometer design of the KAGRA gravitational wave detector. *Phys. Rev.*, D88(4):043007, 2013.
- [56] T. Akutsu et al. Construction of KAGRA: an Underground Gravitational Wave Observatory. *PTEP*, 2018(1):013F01, 2018.
- [57] Zuzanna Kostrzewa-Rutkowska, Łukasz Wyrzykowski, Matthew W. Auger, Thomas E. Collett, and Vasily Belokurov. The evolution of late-type galaxies from CASSOWARY lensing systems. *MNRAS*, 441(4):3238–3248, July 2014.
- [58] S. Birrer et al. H0LiCOW - IX. Cosmographic analysis of the doubly imaged quasar SDSS 1206+4332 and a new measurement of the Hubble constant. *Mon. Not. Roy. Astron. Soc.*, 484:4726, 2019.
- [59] Thomas E. Collett and Matthew W. Auger. Cosmological constraints from the double source plane lens SDSSJ0946+1006. *MNRAS*, 443(2):969–976, September 2014.
- [60] Geoff C. F. Chen, Christopher D. Fassnacht, Sherry H. Suyu, Cristian E. Rusu, James H. H. Chan, Kenneth C. Wong, Matthew W. Auger, Stefan Hilbert, Vivien Bonvin, Simon Birrer, Martin Millon, Léon V. E. Koopmans, David J. Lagattuta, John P. McKean, Simona Vegetti, Frederic Courbin, Xuheng Ding, Aleksii Halkola, Inh Jee, Anowar J. Shajib, Dominique Sluse, Alessandro Sonnenfeld, and Tommaso Treu. A SHARP view of H0LiCOW: H_0 from three time-delay gravitational lens systems with adaptive optics imaging. *MNRAS*, 490(2):1743–1773, December 2019.
- [61] Simon Birrer and Adam Amara. Lenstronomy: multi-purpose gravitational lens modelling software package. 2018.
- [62] James Nightingale, Simon Dye, and Richard J. Massey. AutoLens: automated modeling of a strong lens’s light, mass, and source. *Mon. Not. Roy. Astron. Soc.*, 478(4):4738–4784, 2018.
- [63] Rico Lo et al. In preparation.

- [64] K. Liao, X.-L. Fan, X. Ding, M. Biesiada, and Z.-H. Zhu. Precision cosmology from future lensed gravitational wave and electromagnetic signals. *Nature Communications*, 8:1148, October 2017.
- [65] Bernard F. Schutz. Determining the Hubble Constant from Gravitational Wave Observations. *Nature*, 323:310–311, 1986.
- [66] Max Foxley-Marrable, Thomas E. Collett, Georgios Vernardos, Daniel A. Goldstein, and David Bacon. The impact of microlensing on the standardization of strongly lensed Type Ia supernovae. *Mon. Not. Roy. Astron. Soc.*, 478(4):5081–5090, 2018.
- [67] Masamune Oguri. Strong gravitational lensing of explosive transients. *Rept. Prog. Phys.*, 82(12):126901, 2019.
- [68] Diego, J. M., Hannuksela, O. A., Kelly, P. L., Pagano, G., Broadhurst, T., Kim, K., Li, T. G. F., and Smoot, G. F. Observational signatures of microlensing in gravitational waves at LIGO/Virgo frequencies. *A&A*, 627:A130, 2019.
- [69] Ryuichi Takahashi and Takashi Nakamura. Wave effects in gravitational lensing of gravitational waves from chirping binaries. *Astrophys. J.*, 595:1039–1051, 2003.
- [70] Katerina Chatziioannou, Nicolás Yunes, and Neil Cornish. Model-independent test of general relativity: An extended post-einsteinian framework with complete polarization content. *Phys. Rev. D*, 86:022004, Jul 2012.
- [71] Susmita Adhikari, Maya Fishbach, Daniel E. Holz, Risa H. Wechsler, and Zhanpei Fang. The binary-host connection: astrophysics of gravitational wave binaries from their host galaxy properties. 1 2020.
- [72] B. P. Abbott et al. Instrument Science White Paper2018. 2016. <https://dcc.ligo.org/LIGO-T1800133>.
- [73] Daniel J. Mortlock, Stephen M. Feeney, Hiranya V. Peiris, Andrew R. Williamson, and Samaya M. Nissanke. Unbiased Hubble constant estimation from binary neutron star mergers. *Phys. Rev.*, D100(10):103523, 2019.
- [74] Kenta Hotokezaka, Ehud Nakar, Ore Gottlieb, Samaya Nissanke, Kento Masuda, Gregg Hallinan, Kunal P. Mooley, and Adam.T. Deller. A Hubble constant measurement from superluminal motion of the jet in GW170817. *Nat. Astron.*, 3(10):940–944, 2019.